Research on Chemical Intermediates
https://doi.org/10.1007/s11164-026-05999-w

Amino acid–functionalized magnetic Fe_3O_4 nanocatalysts in aldol addition reactions: a systematic study using full factorial experimental design

Asmar Taghiyeva[1] · Hasniye Yaşa[2] · Mustafa Fatih Ergin[3]

Received: 13 January 2026 / Accepted: 6 April 2026
© The Author(s) 2026

Abstract

Aldol reactions constitute one of the most fundamental carbon–carbon bond-forming transformations in organic synthesis and play a crucial role in the preparation of value-added chemical intermediates. In this study, magnetic Fe_3O_4 nanocatalysts functionalized with two different amino acids were synthesized and evaluated as efficient heterogeneous catalysts for aldol addition reactions. The prepared nanocatalysts were comprehensively characterized by X-ray diffraction (XRD), Fourier transform infrared spectroscopy (FTIR), scanning electron microscopy (SEM), and BET surface area analysis, confirming successful surface functionalization and preservation of the magnetic core structure.The catalytic performance of the amino acid-functionalized Fe_3O_4 nanocatalysts was investigated in model aldol reactions involving cyclohexanone and 4-n-propylcyclohexanone with various aromatic aldehydes. A full factorial experimental design was employed to systematically evaluate the effects of catalyst type and reaction parameters on yield and selectivity, enabling the identification of significant main effects and interaction-driven substrate–catalyst matching behavior. Statistical analysis revealed that catalyst identity and ketone–catalyst interactions play a dominant role in governing reaction efficiency.Under optimized conditions, a series of β-hydroxy ketones were obtained in high isolated yields, including three previously unreported compounds. The magnetic nanocatalysts could be readily recovered using an external magnetic field and reused over multiple reaction cycles with only a minor decrease in catalytic activity. Overall, this study demonstrates that amino acid-functionalized magnetic Fe_3O_4 nanocatalysts, combined with a structured Design of Experiments approach, provide an effective and reliable platform for the synthesis of aldol-type chemical intermediates.

Keywords Aldol reaction · β-hydroxy ketones · Magnetic nanocatalyst · Chemical · Heterogeneous catalysis · DoE

Extended author information available on the last page of the article

Published online: 15 April 2026

Introduction

Aldol reactions are among the most fundamental and extensively investigated carbon–carbon bond-forming transformations in organic chemistry. Owing to their versatility, these reactions play a central role in the synthesis of natural products, pharmaceuticals, and value-added chemical intermediates, making them highly relevant from both academic and industrial perspectives [1]. The development of efficient catalytic systems for aldol reactions remains an active research area, as catalysts can significantly influence reaction efficiency, selectivity, and operational conditions while simultaneously reducing energy consumption and waste generation [2].

Traditionally, aldol condensations have been performed using homogeneous basic catalysts such as NaOH and KOH, particularly in industrial processes. However, these systems often suffer from drawbacks including poor selectivity, difficult product separation, catalyst waste generation, and limited recyclability. To overcome these limitations, extensive efforts have been devoted to alternative catalytic approaches, including heterogeneous catalysts [3], synthetic chiral catalysts [4], biocatalysts [5], and biomimetic systems [6–8]. In parallel, green chemistry strategies, such as solvent-free conditions [9, 10], aqueous media [11], supercritical fluids [12–14], and ionic liquids [15, 16], have been explored to improve the sustainability of aldol processes.

In recent years, nanostructured materials have emerged as attractive catalytic platforms due to their high surface-to-volume ratios and tunable surface properties [17–19]. Among them, spinel magnetic ferrite nanoparticles, particularly Fe_3O_4, have gained considerable attention owing to their low cost, chemical stability, and facile recovery using an external magnetic field [20, 21]. Surface functionalization of Fe_3O_4 nanoparticles with organic ligands, including amino acids, has further expanded their applicability in catalysis by combining the advantages of heterogeneous supports with organocatalytic activity [22, 23]. Amino acid-based organocatalysts are especially appealing due to their structural simplicity, low toxicity, and ability to promote carbon–carbon bond formation under mild conditions.

Alongside catalyst development, the rational optimization of reaction parameters has become increasingly important in contemporary chemical research. Since raw material costs constitute a significant portion of overall production expenses, statistical experimental design methodologies, particularly Design of Experiments (DoE), have gained prominence as powerful tools for process optimization [24]. Unlike conventional one factor at a time approaches, DoE enables the simultaneous evaluation of multiple variables and their interactions, allowing reliable identification of optimal conditions with a reduced number of experiments [25].

Despite significant progress in both amino acid-based organocatalysis and magnetic nanoparticle-supported catalysts, studies that integrate systematic statistical experimental design with detailed analysis of substrate–catalyst interactions in aldol reactions remain relatively scarce. In particular, the application of full factorial design to quantitatively resolve interaction-driven selectivity in

heterogeneous aldol catalysis has not been sufficiently explored. Addressing this gap is essential for gaining deeper mechanistic insight into multicomponent catalytic systems in which reaction performance is governed not only by individual factors but also by complex interaction effects.

Unlike many previous studies that focus primarily on catalyst synthesis or isolated reaction optimization, the present work integrates heterogeneous organocatalysis with a statistically structured full factorial design. This approach enables the quantitative identification of interaction-driven catalytic behavior and provides insight into substrate–catalyst matching effects in aldol reactions. Such statistically resolved analysis remains relatively rare in heterogeneous organocatalytic systems.

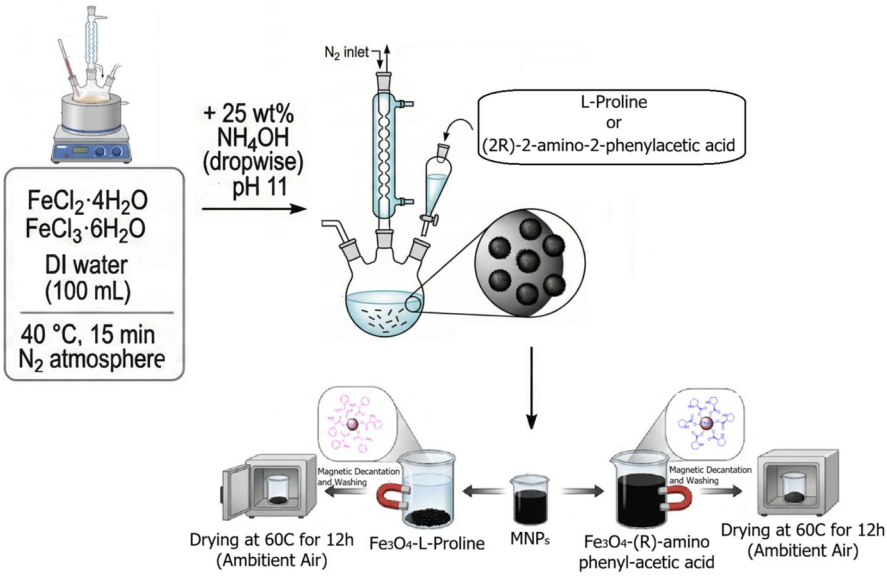
In this study, magnetic Fe_3O_4 nanocatalysts functionalized with two different amino acids (denoted as **3c** and **3e**) were synthesized and comprehensively characterized using X-ray diffraction (XRD), Fourier transform infrared spectroscopy (FTIR), scanning electron microscopy (SEM), and BET surface area analysis. These nanocatalysts were subsequently applied to model aldol addition reactions. A full factorial experimental design was employed to evaluate the effects of key reaction parameters on yield and selectivity, enabling a systematic assessment of individual factors and their interactions. This statistical framework allowed the quantitative identification of interaction-driven catalytic behavior within the investigated multicomponent reaction system. Under statistically optimized conditions, a series of β-hydroxy ketones were obtained in high isolated yields, including three previously unreported compounds (4d, 4e, and 4f). In addition, the magnetic nanocatalyst 3c demonstrated good reusability over multiple reaction cycles. Full experimental procedures together with detailed spectroscopic characterization data for all synthesized compounds are provided in the Supporting Information (Figs. S8–S28).

Materials and methods

Materials

All chemicals were purchased from Merck, Acros, or Aldrich and used as received unless otherwise specified. Reactions were monitored by thin-layer chromatography (TLC) on silica gel plates and visualized under UV light. The products were purified by flash column chromatography on silica gel (Merck, 230–400 mesh) using hexane/ethyl acetate (8:1 or 8:3, v/v) as the eluent. Newly synthesized compounds were purified by column chromatography and characterized by IR, ^{1}H NMR, ^{13}C NMR, elemental analysis, and GC–MS. NMR spectra were recorded on a 500 MHz spectrometer (^{1}H at 500 MHz and ^{13}C at 125 MHz) using tetramethylsilane (Me_4Si) as an internal standard in $CDCl_3$.

GC–MS analyses were carried out using a Shimadzu GC-2010 gas chromatograph coupled with a Shimadzu QP2010 mass spectrometer. Separation was achieved on a TRB-5MS fused silica capillary column (30 m × 0.25 mm i.d., 0.25 μm film thickness). The oven temperature program was as follows: initial temperature 80 °C, increased at a rate of 10 °C min^{-1} to 275 °C and held for 5 min, followed by a further increase at 10 °C min^{-1} to 300 °C and held for 3 min. The mass



Scheme 1 Preparation of amino acid–functionalized magnetic Fe_3O_4 nanocatalysts (**3c** and **3e**)

spectrometer operated in electron impact (EI) mode at an ionization energy of 70 eV with a scan range of 40–550 amu and a scan rate of 0.20 s per scan. The injector, interface, and ion source temperatures were maintained at 250, 275, and 250 °C, respectively. Samples were injected in split mode (1 µL injection volume, split ratio 1:10) using helium as the carrier gas at a flow rate of 1.0 mL min^{-1}. Infrared (IR) spectra were recorded on a Shimadzu IRTracer-100 FT-IR spectrometer. Mass spectra were recorded in electron impact mode (70 eV) and the most abundant fragment ions (m/z) are reported in the Supporting Information.

Methods

Preparation of Fe_3O_4–amino acid nanoparticles

The synthetic procedure employed for the preparation of the magnetic nanocatalysts is schematically presented in Scheme 1. Initially, $FeCl_2 \cdot 4H_2O$ (0.2 g) and $FeCl_3 \cdot 6H_2O$ (0.54 g) were dissolved in 100 mL of deionized water under a nitrogen atmosphere and stirred vigorously at 40 °C for 15 min to ensure complete dissolution of the iron salts. The Fe^{2+}/Fe^{3+} molar ratio was maintained at 1:2, a condition known to favor the formation of the inverse spinel Fe_3O_4 phase during subsequent precipitation.

Following dissolution, 0.3 g of either L-proline or (2*R*)-2-amino-2-phenylacetic acid was introduced into the reaction mixture. A 25 wt% NH_4OH solution was then added dropwise under continuous stirring until the pH reached approximately 11, resulting in the rapid formation of a black suspension characteristic of magnetite

nanoparticle precipitation. Under these strongly alkaline conditions, Fe_3O_4 nanoparticles formed via a co-precipitation mechanism, while the amino acid molecules present in the medium simultaneously interacted with the growing nanoparticle surface. In particular, the carboxylate functionalities of the amino acids are likely to coordinate with surface Fe^{3+} sites during nucleation and growth, thereby enabling in situ surface functionalization of the magnetic particles.

To promote crystallization and facilitate stable anchoring of the organic ligands, the suspension was subsequently heated to 100 °C and maintained under vigorous stirring for 6 h in a nitrogen atmosphere. The inert environment was preserved throughout both the precipitation and growth stages in order to minimize oxidation of Fe^{2+} species and maintain the magnetite phase stability.

After completion of the reaction, the resulting Fe_3O_4–amino acid nanoparticles were isolated by magnetic decantation. The particles were washed three times with distilled water until the washings reached neutral pH and were then dried at 60 °C for 12 h. All synthesis steps prior to the drying stage were conducted under nitrogen, whereas the final drying step was carried out under ambient atmospheric conditions [23, 26].

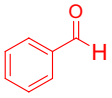
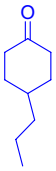
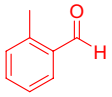
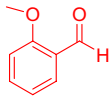
Experimental design and statistical analysis

Reducing raw material costs and enhancing product efficiency are central objectives in industrial catalytic process optimization. Unlike conventional one-factor-at-a-time (OFAT) approaches, statistical Design of Experiments (DoE) enables simultaneous evaluation of multiple variables and their interactions, thereby providing deeper mechanistic insight into complex reaction systems. In this study, a General Full Factorial Design ($2 \times 3 \times 6$) was implemented to systematically investigate substrate–catalyst interactions and optimize reaction yield [27–29].

All statistical analyses were conducted using Minitab® 19 software. Three independent variables were examined: ketone derivative (2 levels: **1a–1b**), aldehyde derivative (3 levels: **2a–2c**), and catalyst type (6 levels: **3a–3f**), as summarized in Table 1. The chemical structures of all ketone substrates, aldehyde derivatives, and catalysts included in the factorial design are illustrated in Scheme 2, allowing clear identification of the molecular components investigated in the factorial design study. A total of 36 experimental runs were performed in randomized order to minimize uncontrolled environmental bias. Replication was intentionally omitted to maximize coverage of the multicomponent design space within the available experimental framework, consistent with exploratory factorial optimization strategies. The design aimed to explore a broad reaction space rather than estimate experimental variance.

Table 1 Factors and levels used in the full factorial experimental design

Factor	Levels	Values
Ketone derivatives	2	1a, 1b
Aldehyde derivatives	3	2a, 2b, 2c
Catalyst	6	3a, 3b, 3c, 3d, 3e, 3f

Ketone Substrates	Aldehyde Substrates	Catalyst
 **(1a)**	 **(2a)**	K_2CO_3 **(3a)**
		L-proline **(3b)**
 **(1b)**	 **(2b)**	Fe_3O_4-L-proline **(3c)**
		Fe_3O_4-L-proline + Benzoic acid **(3d)**
		Fe_3O_4-(2*R*)-2-amino-2-phenylacetic acid **(3e)**
	 **(2c)**	Fe_3O_4-(2*R*)-2-amino-2-phenylacetic acid + Benzoic acid **(3f)**

Scheme 2 Chemical structures of the ketone substrates (1a–1b), aromatic aldehyde derivatives (2a–2c), and catalytic systems (3a–3f) investigated in the full factorial Design of Experiments (DoE) study

Replication was intentionally omitted in order to maximize coverage of the multicomponent design space within the available experimental framework. This strategy is commonly applied in exploratory factorial studies involving multiple discrete factors. In such cases, experimental error can be estimated by pooling statistically insignificant higher-order interactions.

Accordingly, the error term for ANOVA was obtained by pooling the three-way interaction ($A \times B \times C$), which was found to be statistically insignificant. Pooling higher-order interactions to estimate residual variance is a widely accepted practice in unreplicated factorial designs when such interactions are negligible [27], allowing reliable estimation of experimental error.

Model adequacy was evaluated through comprehensive residual diagnostics, including normal probability plots, residual-versus-fitted analysis, leverage statistics, and Cook's distance. The Anderson–Darling test confirmed the normal distribution of residuals ($p > 0.05$), and no evidence of heteroscedasticity or influential observations was detected. Model robustness and predictive capability were assessed using the coefficient of determination (R^2), adjusted R^2 (R^2_adj), and predicted R^2 (R^2_pred). The close agreement between predicted and experimentally validated optimal yields further confirms the reliability of the factorial model.

To quantify factor influence, the percentage contribution of each term to the total sum of squares was calculated. Catalyst identity emerged as the dominant factor, accounting for 64.7% of the total variance in reaction yield. The ketone × catalyst interaction contributed 25.5%, while the aldehyde main effect accounted for 8.3%. In contrast, the ketone main effect alone was statistically negligible (< 0.1%). Overall,

more than 90% of the explained variability arises from catalyst-driven effects and substrate–catalyst interactions, indicating that the reaction outcome is governed primarily by interaction-dependent catalytic selectivity rather than simple linear factor contributions. This statistical structure is consistent with strong substrate–catalyst matching behavior within the investigated catalytic system.

General procedure for the aldol reaction

In a single-neck round-bottom flask equipped with a magnetic stir bar, ketone (0.10 mmol) and aldehyde (0.5 mmol) were dissolved in a mixture of DMSO:H_2O (8:2, v/v, 3 mL). Subsequently, the magnetic nanocatalyst (0.03 g, corresponding to 30 mol%) was added, and the reaction mixture was stirred at room temperature for 72 h. All synthesis steps prior to the drying stage were conducted under nitrogen, whereas the final drying step was carried out under ambient atmospheric conditions [23, 26].

The progress of the reaction was monitored by thin-layer chromatography (TLC). Upon completion, the reaction mixture was washed once with saturated aqueous NaCl solution and transferred to a separatory funnel. The aqueous phase was extracted three times with ethyl acetate (EtOAc). The combined organic layers were dried over anhydrous Na_2SO_4, filtered, and concentrated under reduced pressure using a rotary evaporator [7, 30].

Reaction monitoring was performed by TLC, and spots were visualized under UV light. Isolated yields were determined after purification by flash column chromatography on silica gel (Merck, 230–400 mesh), using hexane/ethyl acetate mixtures (v/v 8:1 or 8:3) as the mobile phase. The spectroscopic data of compounds 4a–4f are provided in the Supporting Information (Figs. S8–S10 for 4a, S11–S13 for 4b, S14–S16 for 4c, S17–S20 for 4d, S21–S24 for 4e, and S25–S28 for 4f).

Result and discussion

Catalyst characterization

The synthesized magnetic nanoparticles were comprehensively characterized using X-ray diffraction (XRD), Fourier transform infrared spectroscopy (FTIR), Brunauer–Emmett–Teller (BET) surface area analysis, scanning electron microscopy (SEM), and energy-dispersive X-ray spectroscopy (EDX) techniques.

XRD analysis

The crystalline structure of Fe_3O_4, Fe_3O_4–L-proline (**3c**), and Fe_3O_4–(2*R*)-2-amino-2-phenylacetic acid (**3e**) nanoparticles was examined by X-ray diffraction (Fig. 1). The diffraction patterns of the functionalized samples closely resemble that of pristine Fe_3O_4, indicating that the spinel ferrite structure of the magnetic core was preserved during amino acid immobilization. Additional X-ray diffraction (XRD)

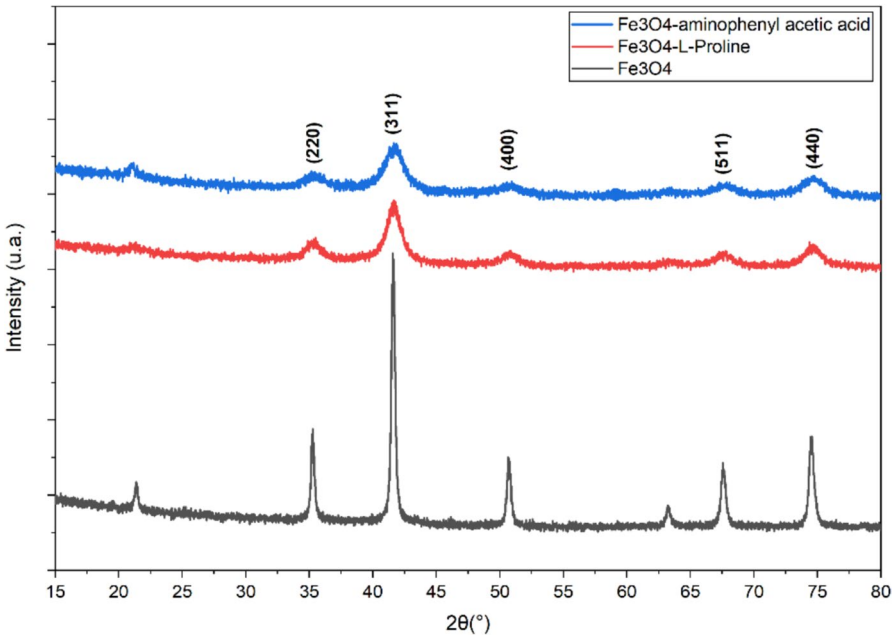


Fig. 1 XRD patterns of pristine Fe_3O_4, Fe_3O_4–L-proline (**3c**), and Fe_3O_4-(2*R*)-2-Amino-2-phenylacetic acid (**3e**) magnetic nanoparticles recorded using Cu Kα radiation

patterns of the fresh and recovered catalysts are provided in the Supporting Information (Fig. S6). The comparison of these patterns confirms that the characteristic diffraction peaks of the spinel Fe_3O_4 structure remain unchanged after the catalytic cycles, indicating the structural stability of the magnetic nanocatalyst.

The characteristic reflections observed at 2θ values of approximately 30.1, 35.5, 43.2, 57.1, and 62.6 correspond to the (220), (311), (400), (511), and (440) crystallographic planes of Fe_3O_4 respectively [22, 23], which are in good agreement with the standard magnetite pattern (JCPDS card No. 19-0629). The absence of additional diffraction peaks confirms that no secondary crystalline phases were generated during the functionalization process.

A slight reduction in peak intensity together with moderate peak broadening was observed for the functionalized samples. This behavior can be attributed to the presence of an amorphous organic coating layer on the nanoparticle surface, which partially attenuates the diffraction signal without altering the crystalline structure of the magnetite core.

The average crystallite size of the synthesized magnetic nanoparticles was estimated using the Scherrer equation:

$$D = K\lambda / (\beta \cos\theta) \quad (1)$$

where D is the crystallite size, K is the shape factor (0.9), λ is the X-ray wavelength (0.15406 nm for Cu Kα radiation), β is the full width at half maximum (FWHM) of

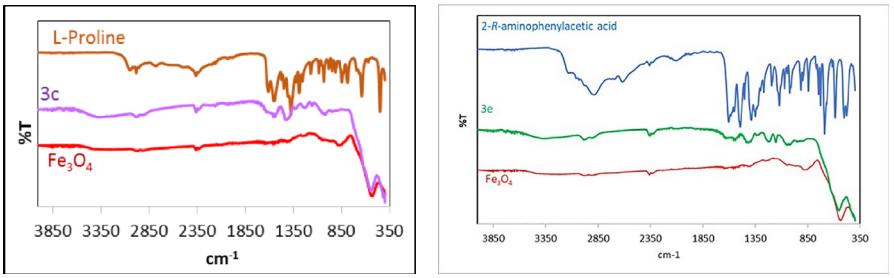
the diffraction peak, and θ is the Bragg diffraction angle. The crystallite size calculated from the most intense (311) reflection was approximately 7–9 nm, confirming the nanocrystalline nature of the Fe_3O_4-based catalysts.

FTIR analysis

The FT-IR spectrum of L-proline showed bands at 1608 and 1375 cm^{-1}, corresponding to the asymmetric and symmetric stretching of the carboxylate (COO^-) group, and a band at 1550 cm^{-1} due to N–H bending of the secondary amine. The 1290–1031 cm^{-1} region exhibited C–N and C–O stretching vibrations, while the absence of a distinct O–H stretch supports the zwitterionic form in the solid state [31].

For (2R)-2-amino-2-phenylacetic acid, the C=O stretch appeared at 1610 cm^{-1}, accompanied by aromatic C=C bands (1581–1350 cm^{-1}) and N–H stretching at 3125 cm^{-1}. C–N and C–O vibrations were observed in the 1120–1031 cm^{-1} range.

After immobilization onto Fe_3O_4 (samples **3c** and **3e**), these characteristic bands become weaker and slightly shifted. The attenuation of $\nu(COO^-)$ and ν(N–H) bands suggests coordination of the amino acid functional groups to surface Fe centers. In both **3c** and **3e**, the strong Fe–O stretching band at ~ 570–600 cm^{-1} confirms the presence of the magnetic core. Although the organic bands are less intense due to the dominant inorganic phase, the observed shifts and band modifications clearly indicate successful surface functionalization [22, 23]. Additional FTIR spectra of the fresh and reused catalysts are provided in the Supporting Information (Figure S7). The comparison of the spectra demonstrates that the characteristic bands associated with the amino acid ligands and the Fe–O vibrations remain unchanged after the catalytic cycles, confirming the chemical stability of the functionalized magnetic nanocatalyst.(Fig. 2)



(a) **(b)**

Fig. 2 FTIR spectra of Fe_3O_4, L-proline, and Fe_3O_4–L-proline (**3c**) (**a**), Fe_3O_4, ((2*R*)-2-amino-2-phenylacetic acid, and Fe_3O_4-(2*R*)-2-amino-2-phenylacetic acid (**3e**) (**b**)

SEM and EDX analysis

The morphology and surface characteristics of the synthesized magnetic nanocatalysts were investigated using scanning electron microscopy (SEM) (Fig. 3a–c). The micrographs reveal aggregated clusters composed of nanosized particles exhibiting quasi-spherical morphology. Such aggregation behavior is commonly observed for magnetite nanoparticles and arises from strong magnetic dipole–dipole interactions combined with the inherently high surface energy of nanoscale particles.

SEM images show aggregates of nanoparticles with apparent sizes of 20–50 nm, which likely consist of smaller nanocrystallites (7–9 nm) estimated from XRD analysis. The formation of larger aggregates can be attributed to the magnetic nature of Fe_3O_4 particles, which promotes interparticle attraction during drying and sample preparation.

It should be noted that the particle size observed in SEM images may differ from the crystallite size estimated from XRD analysis, since individual nanoparticles can consist of multiple crystalline domains aggregated into larger clusters. The crystallite size calculated from the (311) reflection using the Scherrer equation was approximately 7–9 nm, indicating that the observed SEM particles likely consist of aggregated nanocrystallites.

The elemental composition of the materials was further examined using energy-dispersive X-ray (EDX) spectroscopy (Fig. 3d–e). For sample 3c, the surface composition is dominated by carbon (67.44 wt%) and oxygen (30.29 wt%), while the Fe signal is significantly attenuated (2.27 wt%). This reduced Fe signal can be attributed to the surface-sensitive nature of EDX analysis together with the presence of an organic ligand layer coating the magnetic nanoparticles. The elemental composition of the synthesized catalysts was confirmed by energy-dispersive X-ray (EDX)

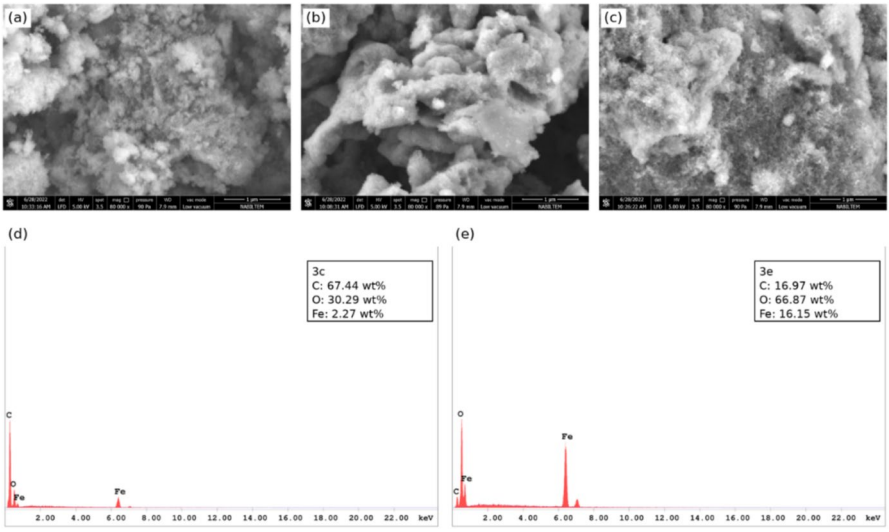


Fig. 3 SEM (**a**–**c**) and EDX (**d**–**e**) analyses of Fe_3O_4-based magnetic nanocatalysts

analysis. The corresponding EDX spectra are provided in the Supporting Information (Fig. S4–S5).

Similarly, sample **3e** exhibits pronounced carbon and oxygen signals together with characteristic Fe peaks, confirming the presence of organic functional groups on the nanoparticle surface. The attenuation of the Fe signal relative to pristine Fe_3O_4 supports the formation of an organic ligand shell surrounding the magnetic core. Collectively, the SEM and EDX analyses confirm the successful surface functionalization of Fe_3O_4 nanoparticles with amino acid ligands.

BET surface analysis

BET measurements were performed to investigate the textural properties of the magnetic nanocatalysts (Fig. 4). The nitrogen adsorption–desorption isotherms indicate that surface functionalization significantly modifies the surface characteristics of Fe_3O_4 nanoparticles. The textural properties of the synthesized catalysts were investigated by nitrogen adsorption–desorption analysis. The BET adsorption–desorption isotherms of Fe_3O_4 and the amino acid–functionalized catalysts are provided in the Supporting Information (Fig. S1–S3).

The specific surface area of pristine Fe_3O_4 (11.07 $m^2\ g^{-1}$) decreases to 5.76 $m^2\ g^{-1}$ and 5.27 $m^2\ g^{-1}$ after modification with L-proline [32] and (2*R*)-2-amino-2-phenylacetic acid, respectively. This reduction in surface area can be attributed to partial surface coverage and pore blocking caused by the immobilized organic ligands.

Despite the decrease in BET surface area, the catalytic activity of the functionalized materials increased significantly. This observation suggests that catalytic performance is governed primarily by the chemical nature and accessibility of surface functional groups rather than by the total accessible surface area alone. The

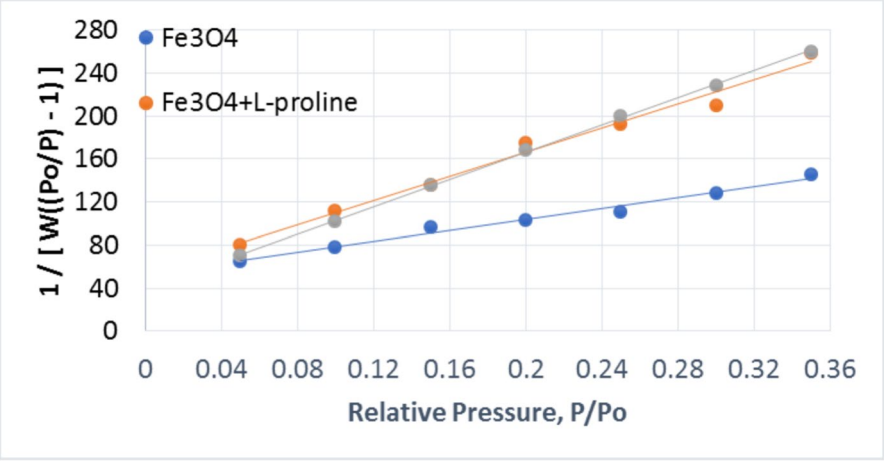


Fig. 4 BET adsorption analysis of pristine Fe_3O_4 and surface-functionalized Fe_3O_4-based magnetic nanocatalysts

increased BET C constant observed after functionalization indicates stronger adsorbate–surface interactions, which can be attributed to the presence of amino acid functionalities that enhance substrate adsorption and facilitate catalytic activation.

These results suggest that surface functionalization generates more defined catalytic microenvironments on the Fe_3O_4 surface, thereby improving substrate–catalyst interactions and contributing to the enhanced catalytic performance observed in the aldol reaction.

Catalytic activity and full factorial experimental dataset

Following structural and surface characterization, the catalytic performance of all catalyst–substrate combinations was systematically evaluated using a $2 \times 3 \times 6$ full factorial experimental design. In total, 36 experiments were conducted to examine the effects of ketone type, aldehyde derivative, and catalyst identity on aldol reaction yield. The structures of the ketone derivatives (1a–1b), aldehyde substrates (2a–2c), and catalysts (3a–3f) used in the factorial experimental design are summarized in Scheme 2. This scheme provides a visual reference for all reaction components evaluated in the DoE matrix.

The complete experimental dataset obtained from the factorial design is presented in Table 2. This dataset constitutes the primary source of all subsequent statistical analyses, including ANOVA, main effect estimation, interaction analysis, and response optimization.

Statistical evaluation of reaction parameters

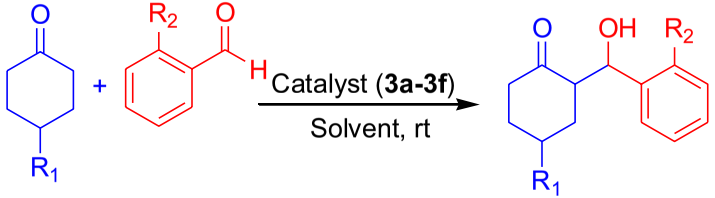
Based on the experimental results summarized in Table 2, statistical analysis was performed using analysis of variance (ANOVA) to determine the significance of individual factors and their interactions.

In preliminary experiments performed under standard reaction conditions, the target aldol product was obtained with a moderate yield of approximately 61%. To systematically improve the reaction performance and quantitatively evaluate the influence of the reaction components, a full factorial experimental design was implemented. The statistical significance of the resulting model was assessed using analysis of variance (ANOVA).

The Pareto chart provides a graphical representation of the relative magnitude of factor effects. However, statistical significance was primarily evaluated based on the ANOVA *p*-values summarized in Table 3. The ranking of effects observed in the Pareto chart is consistent with the ANOVA results, confirming that catalyst identity (C) and the ketone × catalyst interaction (AC) are the dominant contributors to reaction yield.

As summarized in Table 2, the model exhibits a high F-value of 56.20 with a corresponding *p*-value lower than 0.001, indicating that the variation observed in the experimental data is predominantly explained by the factorial model rather than by random experimental error. This result confirms that the selected reaction parameters exert statistically significant effects on the aldol reaction yield.

Table 2 Effect of catalyst type on aldol reaction yield within full factorial design



1a-1b **2a-2c** **4a-4f**

,

Yield[b]							
Product	R_1, R_2	K_2CO_3	L-proline	Fe_3O_4-L-proline	Fe_3O_4-L-proline + Benzoic acid[c]	Fe_3O_4-(2*R*)-2-amino-2-phenylacetic acid	Fe_3O_4- (2*R*)-2-amino-2-phenylacetic acid[c]
		(3a)	(3b)	(3c)	(3d)	(3e)	(3f)
4a	H, H	61	80	81	82	40	45
4b	H, CH_3	68	85	87	88	46	50
4c	H, OCH_3	60	78	75	77	36	38
4d	C_3H_7, H	67	70	65	67	61	62
4e	C_3H_7, CH_3	70	76	76	78	60	64
4f	C_3H_7, OCH_3	62	67	62	64	57	59

[a]Reaction conditions: aromatic aldehyde (0.5 mmol), cyclohexanone (0.1 mmol), catalyst (0.03 g) are stirred DMSO:H_2O (8:2, v/v, 3 mL) at room temperature for 3 days

[b]Isolated yield

[c]Reaction conditions: aromatic aldehyde (0.5 mmol), cyclohexanone (0.1 mmol), and catalyst (3c or 3e, 0.03 g) in the presence of benzoic acid (5 mol%) were stirred in DMSO (1 mL) at room temperature for 3 days

Table 3 Analysis of variance (ANOVA) results for the factorial model evaluating the effects of ketone derivative, aldehyde derivative, and catalyst type on aldol reaction yield

Source	DF	Adj SS	Adj MS	F-Value	*P* Value
Model	25	6408.39	256.336	56.20	< 0.001
Linear	8	4714.28	589.285	129.20	< 0.001
Ketone derivatives	1	2.78	2.778	0.61	0.453
Aldehyde derivatives	2	538.17	269.083	59.00	< 0.001
Catalyst	5	4173.33	834.667	183.00	< 0.001
2-Way Interactions	17	1694.11	99.654	21.85	< 0.001
Ketone derivatives*Aldehyde derivatives	2	2.06	1.028	0.23	0.802
Ketone derivatives*Catalyst	5	1644.56	328.911	72.11	< 0.001
Aldehyde derivatives*Catalyst	10	47.50	4.750	1.04	0.475
Error	10	45.61	4.561		
Total	35	6454.00			

A detailed examination of the ANOVA results reveals that catalyst identity represents the most influential factor affecting the reaction outcome ($p < 0.001$). The aldehyde derivative also shows a statistically significant contribution ($p < 0.001$). In contrast, the main effect of the ketone derivative was statistically insignificant ($p = 0.453$), suggesting that the ketone structure alone does not strongly influence the reaction yield under the investigated conditions.

Interaction effects between the experimental factors were also evaluated. Among the examined interactions, the ketone × catalyst interaction exhibits a highly significant effect ($p < 0.001$), indicating that catalytic performance strongly depends on the specific substrate–catalyst combination. In contrast, the ketone × aldehyde interaction and aldehyde × catalyst interaction were statistically insignificant, suggesting that these parameter combinations exert only a limited influence on reaction efficiency.

The adequacy and robustness of the factorial model were further validated through residual diagnostics. Normal probability plots of the residuals confirmed that the data do not deviate from the assumption of normality, as supported by the Anderson–Darling test ($p > 0.05$). Moreover, residual-versus-fitted plots revealed no discernible patterns, confirming that the assumption of variance homogeneity (homoscedasticity) was satisfactorily satisfied. Additional diagnostic indicators, including Cook's distance and leverage values, indicated that no influential observations disproportionately affected the model predictions.

The explanatory power of the model is remarkably high, with a coefficient of determination (R^2) of 99.29%, an adjusted R^2 value of 97.53%, and a predicted coefficient of determination (R^2_pred) of 90.84% (Table 4). The close agreement between the

Table 4 Summary of model statistics

S	R-sq	R-sq(adj)	R-sq(pred)
2.13568	99.29%	97.53%	90.84%

adjusted and predicted R^2 values indicates that the model possesses strong predictive capability without evidence of overfitting.

Overall, these statistical results demonstrate that the developed factorial model provides a reliable and robust framework for evaluating the effects of reaction parameters on aldol reaction efficiency. The findings further highlight the dominant role of catalyst identity and catalyst–substrate interactions in controlling the performance of the catalytic system.

Identification of significant factors affecting reaction yield

To identify the factors governing the reaction performance, the Pareto chart of standardized effects was examined (Fig. 5). This graphical analysis highlights the magnitude and statistical significance of the model terms based on the standardized effect values. The vertical reference line corresponds to the 95% confidence limit, indicating the threshold above which effects are considered statistically significant.

Among the investigated parameters, the catalyst type (C) clearly represents the most dominant factor affecting the reaction yield. The ketone × catalyst interaction (AC) also exceeds the significance threshold, indicating a strong interaction between the substrate and the catalytic system. The aldehyde derivative (B) shows a statistically significant but comparatively smaller effect. In contrast, the ketone derivative (A) and the remaining interaction terms fall below the confidence limit and therefore do not exert a statistically meaningful influence within the experimental domain investigated.

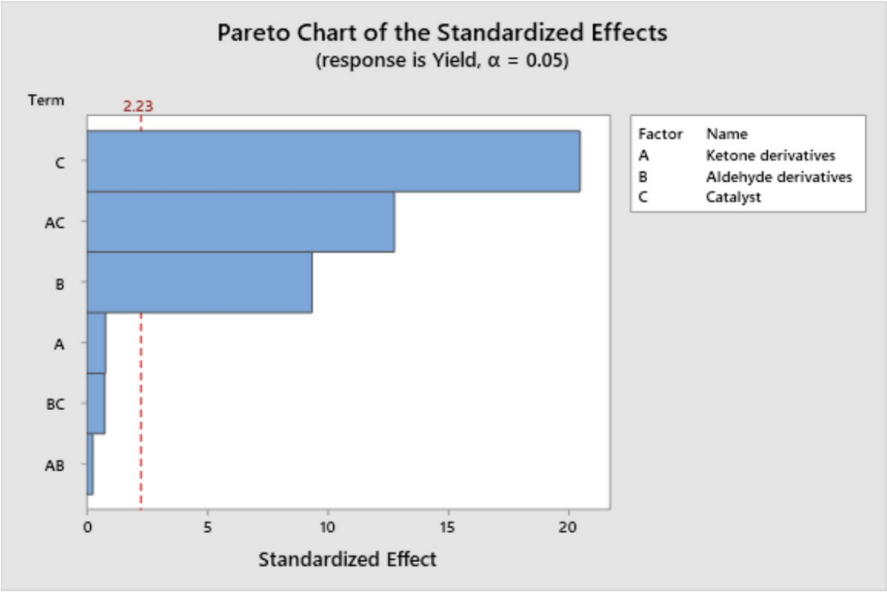


Fig. 5 Pareto chart of standardized effects for the factorial model

These findings indicate that catalytic identity plays the primary role in determining the efficiency of the aldol reaction, while substrate–catalyst interactions also contribute significantly to the observed variability in reaction yield.

Main effects of reaction parameters on yield

The main effects plots shown in Fig. 6 illustrate the average influence of each factor level on the reaction yield.

Only a minor difference in yield was observed between the two ketone derivatives (**1a** and **1b**), indicating that the ketone structure alone does not strongly affect the reaction outcome. This observation is consistent with the ANOVA results, which identified the ketone main effect as statistically insignificant.

In contrast, the aldehyde derivatives exhibit a more pronounced influence on reaction yield. Among the tested substrates, aldehyde **2b** produced the highest average yield, whereas **2c** resulted in noticeably lower conversion. These differences suggest that electronic and steric characteristics of the aldehyde component can affect the reaction efficiency.

The most significant variation is observed within the catalyst series. Catalysts **3b** and **3d** deliver substantially higher yields than the remaining catalysts, indicating their superior catalytic efficiency. Conversely, catalyst **3e** produces markedly reduced yields, while catalyst 3f shows only partial recovery of activity. This

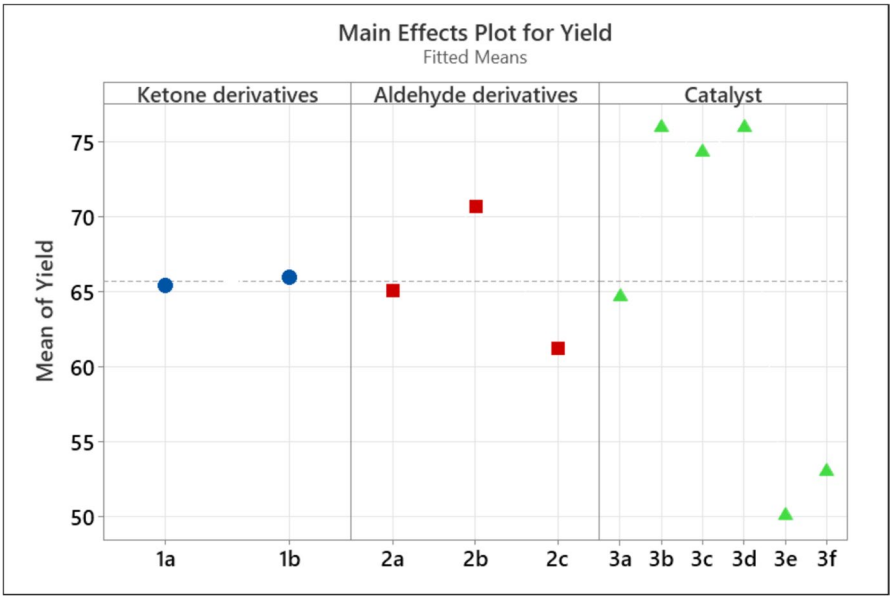


Fig. 6 Main effects plots showing the influence of ketone type, aldehyde derivative, and catalyst on reaction yield

wide variation confirms that catalyst selection is the dominant factor controlling the reaction performance.

Overall, the main effects analysis demonstrates that although substrate identity contributes to reaction variability, the chemical nature and efficiency of the catalyst exert the most decisive influence on the final reaction yield.

Interaction analysis

The interaction plots presented in Fig. 7 provide further insight into the relationships between the experimental factors. According to the ANOVA results, the main effect of the ketone derivative (A) was statistically insignificant ($p = 0.453$), whereas the ketone × catalyst interaction (AC) was highly significant ($p < 0.001$) [32].

This behavior represents a typical interaction-driven response pattern in which the influence of a factor becomes apparent only in combination with another variable. In the present system, the catalytic performance depends strongly on the specific pairing between the ketone substrate and the catalyst [33].

The interaction plots clearly illustrate that although the ketone derivatives exhibit similar average yields when evaluated independently, their behavior changes significantly in the presence of different catalysts. In particular, the combination of ketone **1a** with catalysts **3b** and **3d** produces substantially higher

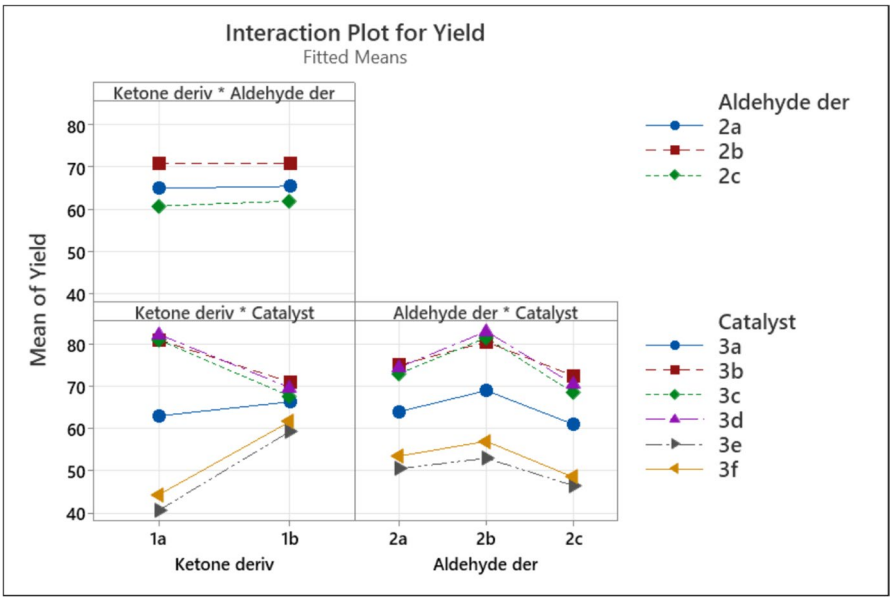


Fig. 7 Interaction plots showing the effects of ketone, aldehyde, and catalyst interactions on reaction yield

yields, whereas catalyst **3e** consistently results in reduced activity. These observations demonstrate that the reaction efficiency is governed by the compatibility between catalyst structure and substrate reactivity [34].

In contrast, the aldehyde × catalyst interaction shows relatively parallel trends, indicating that the influence of aldehyde identity is less dependent on catalyst type. Thus, although aldehyde structure contributes to reaction variability, it does not override the dominant catalytic effect observed in the system.

Overall, the interaction analysis confirms that the reaction yield is primarily controlled by catalyst identity and substrate–catalyst interactions rather than by the isolated effects of individual reaction components.

Response optimization and mechanistic interpretation

The optimal reaction conditions predicted by the factorial model were determined using the particle assemblies appea (Fig. 8). This graphical tool identifies the combination of factor levels that maximizes the predicted response value.

According to the model, the optimal conditions correspond to the combination of ketone **1a**, aldehyde **2b**, and catalyst **3d**. Under these conditions, the predicted maximum reaction yield is 89.61% [35].

To validate the reliability of the statistical model, an experiment was performed under the predicted optimal conditions. The resulting isolated yield of approximately 89% is in excellent agreement with the predicted value, confirming the predictive accuracy and robustness of the developed factorial model.

These results demonstrate that the full factorial design provides an effective strategy for identifying optimal reaction conditions and for understanding the complex interplay between catalyst identity and substrate structure in the aldol reaction system [36–38].

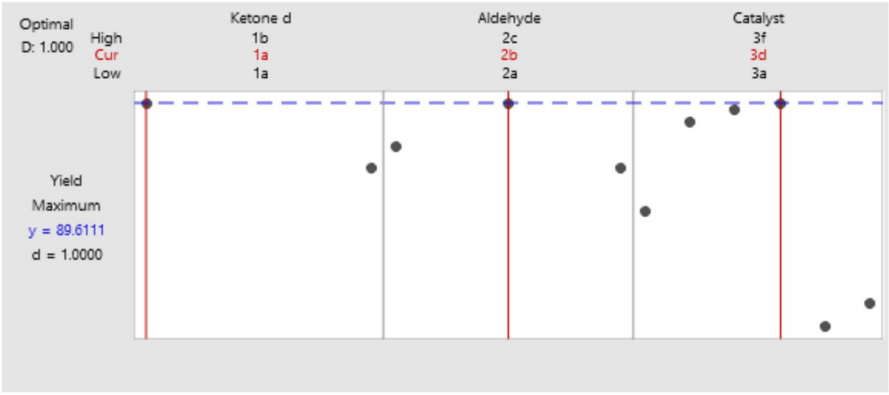


Fig. 8 Response optimizer plot predicting the global maximum yield and corresponding optimal factor levels

Integrated DoE-driven analysis of the catalytic aldol reaction

The efficiency of the aldol addition catalyzed by amino acid–functionalized magnetic Fe_3O_4 nanoparticles is not dictated solely by the intrinsic reactivity of the aldehyde and ketone substrates. Equally important is the degree of compatibility between the catalyst surface and the reacting carbonyl compound. In such multicomponent catalytic systems, conventional one-factor-at-a-time (OFAT) optimization strategies are insufficient because they cannot disentangle the intertwined effects arising from substrate structure and catalyst identity. To address this limitation, a general full factorial experimental design was employed to quantitatively resolve both individual factor effects and interaction-driven contributions governing reaction yield.

The factorial model included three independent variables: ketone identity (**1a–1b**), aldehyde identity (**2a–2c**), and catalyst type (**3a–3f**), resulting in a total of 36 randomized experimental runs (the complete experimental matrix and results are summarized in Table 2). Because the three-way interaction term (A × B × C) was statistically insignificant, it was pooled to estimate experimental error, following a standard approach for unreplicated factorial designs. Analysis of variance (ANOVA) confirmed that the overall model is highly significant ($F = 56.20$, $p < 0.001$) and exhibits excellent explanatory and predictive capability ($R^2 = 99.29\%$, $R^2_adj = 97.53\%$, $R^2_pred = 90.84\%$) (Table 3). These results indicate that the variation in reaction yield is primarily governed by chemically meaningful factors rather than random experimental variability.

Inspection of the Pareto chart of standardized effects together with the ANOVA results reveals that catalyst identity constitutes the dominant main effect controlling the efficiency of the aldol reaction (Fig. 5). This statistical predominance reflects the central chemical role of the catalyst in facilitating carbonyl activation and stabilizing key intermediates involved in C–C bond formation. In contrast, the main effect of ketone identity alone is statistically insignificant ($p = 0.453$). Notably, however, the interaction between ketone identity and catalyst type (A × C) is highly significant ($p < 0.001$), indicating that reaction efficiency depends strongly on the specific pairing between substrate and catalyst.

From a chemical perspective, these findings suggest that ketone reactivity cannot be evaluated independently of the catalyst environment. Although ketones **1a** and **1b** display comparable average yields when considered individually, their performance varies substantially depending on the catalyst employed. The interaction plots clearly show that certain ketone–catalyst combinations lead to pronounced yield enhancement, whereas mismatched combinations result in reduced catalytic efficiency. Such behavior is consistent with a substrate–catalyst matching mechanism in which optimal steric and electronic complementarity facilitates the formation and stabilization of reactive intermediates.

In comparison, aldehyde identity exhibits a statistically significant main effect on reaction yield, with aldehyde **2b** delivering the highest average yields across the catalyst series. This trend suggests that the electronic and steric characteristics of aldehyde **2b** are particularly favorable for the carbon–carbon bond-forming step. Nevertheless, the aldehyde × catalyst interaction (B × C) is relatively weak, indicating that

although aldehyde structure contributes to reaction variability, its influence remains secondary to the dominant catalytic effect.

Response optimization integrates these statistically consistent trends to identify the global optimum reaction conditions. The model predicts that the combination of ketone **1a**, aldehyde **2b**, and catalyst **3d** provides the highest yield, with a predicted maximum of 89.61% (Fig. 6). Experimental validation under these conditions afforded an isolated yield of approximately 89%, in excellent agreement with the model prediction. This close correspondence confirms both the predictive accuracy of the factorial model and the robustness of the applied optimization strategy.

The high catalytic performance observed for catalyst **3d** can be rationalized by considering the modified surface environment created by the benzoic acid functionality. This modification likely tunes the local acid–base balance and hydrogen-bonding interactions at the catalytic interface, thereby promoting efficient carbonyl activation while maintaining sufficient substrate mobility. In contrast, catalysts such as **3e** appear to generate less favorable surface interactions, which may hinder effective substrate activation and consequently reduce catalytic efficiency.

Overall, the combined statistical and chemical analysis demonstrates that the aldol reaction system is governed predominantly by interaction-driven selectivity rather than simple linear factor effects. Consequently, optimal catalytic performance can only be achieved through simultaneous consideration of substrate structure and catalyst identity. The present full factorial Design of Experiments approach therefore provides a powerful framework for unraveling complex catalytic behavior and for rationally identifying optimal catalytic systems in heterogeneous aldol reactions.

These findings highlight the importance of statistically guided catalyst–substrate matching strategies for the rational optimization of heterogeneous aldol catalytic systems.

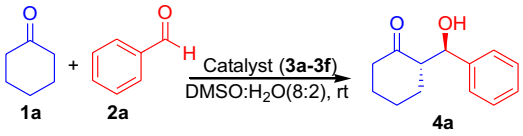
Catalytic activity of nanoparticles

In this study, the following were tested in their aldol performance: as ketones; **1a** and **1b**, as aldehydes; **2a**, **2b,** and **2c**, and as catalysts **3a**, **3b**, **3c**, **3d**, **3e,** and **3f**. Among catalysts used, **3a** and **3b** were commercially available, while **3c** and **3e** were synthesized. The synthesized catalysts were used for the first time in aldol reactions. The results of all the obtained are given in Table 2.

The results obtained from catalysts using **1a** and **2a** as model reactions in DMSO:H_2O (8:2) medium, which is the optimum solvent for the aldol reaction, are shown in Table 5.

To evaluate diastereoselectivity trends independently from the multivariate yield optimization, catalytic performance was assessed under fixed model reaction conditions (**1a**–**2a**, DMSO:H_2O (8:2), 0.03 g catalyst). The resulting anti/syn ratios are summarized in Table 5. The diastereomeric ratios were determined from ^{1}H NMR spectra by integration of proton signals. It should be emphasized that global yield optimization and statistical factor evaluation were performed exclusively through the 36-run full factorial design (Table 2).

Table 5 Diastereoselectivity (anti/syn) for catalysts in the model aldol reaction (**1a–2a**) under fixed conditions



Entry	Catalyst (g)	Yield (%)[b]	dr (anti/syn)[c]
1	**3a**	68	50:50
2	**3b**	85	95:5
3	**3c**	87	94:6
4	**3d**	88	94:6
5	**3e**	46	93:7
6	**3f**	50	91:9

[a]Reaction conditions: aromatic aldehyde (0.5 mmol), cyclohexanone (0.1 mmol), Fe_3O_4–L-proline nanoparticle (0.03 g) are stirred in DMSO:H_2O (8:2, v/v, 3 mL) at room temperature for 3 days

[b]Isolated yield

[c]Anti/syn ratio determined using ^{1}H NMR analysis

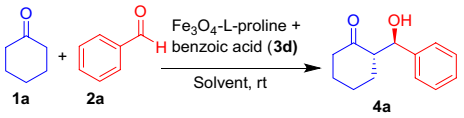
To determine the optimum catalyst loading, the aldol reaction was carried out using 0.01–0.04 g of the **3d** nanocatalyst. The highest yield for β-hydroxy ketone formation (88%) was achieved with a catalyst loading of 0.03 g after three days of reaction time (Table 6). Increasing or decreasing the catalyst amount beyond this level did not lead to any further improvement in the reaction efficiency.

Interestingly, the aldol reaction exhibited a pronounced solvent effect; therefore, the results obtained using different solvents are summarized in Table 6. A wide range of solvents, including polar protic, polar aprotic, and nonpolar solvents, were examined. According to the results presented in Table 6, among the polar protic solvents, methanol afforded a good yield, ethanol resulted in a moderate yield, whereas water led to a relatively low conversion. In contrast, very low yields were obtained when nonpolar solvents such as hexane and toluene were used, as well as when polar aprotic solvents such as acetonitrile and tetrahydrofuran were employed.

The best performance was achieved using a mixed solvent system consisting of DMSO (a polar aprotic solvent) and water (a polar protic solvent) in an 8:2 ratio. This solvent combination provided a significantly enhanced reaction yield compared to the individual solvents. Notably, DMSO in the presence of a small amount of water has been widely preferred for aldol reactions and has been successfully employed in numerous previous studies, owing to its ability to stabilize charged intermediates and facilitate carbon–carbon bond formation [4, 39–41].

A plausible reaction pathway is proposed based on experimental trends and literature precedents, without claiming definitive mechanistic proof (Fig. 9). The mechanism proceeds via classical proline-enamine activation. The role of benzoic

Table 6 The effect of solvent selection and catalyst amount on the aldol reaction



Entry	Catalyst (g)	Solvent	Yield[b]	dr (anti/syn)[c]
1	0.03	EtOH	65	64:36
2	0.03	MeOH	66	75:25
3	0.03	Hexane	12	56:44
4	0.03	THF	65	58:42
5	0.03	Toluene	15	61:39
6	0.03	DMF	68	75:25
7	0.03	DMSO:H_2O(8:2)	74	78:22
8	0.01	DMSO:H_2O(8:2)	62	89:11
9	0.02	DMSO:H_2O(8:2)	74	90:10
10	**0.03**	DMSO:H_2O(8:2)	**82**	94:
11	0.04	DMSO:H_2O(8:2)	82	94:6
12	0.03	H_2O	10	50:50

[a]Reaction conditions: aromatic aldehyde (0.5 mmol), cyclohexanone (0.1 mmol), Fe_3O_4–L-proline nanoparticle (0.03 g) + 5%mol benzoic acid are stirred in DMSO:H_2O (8:2, v/v, 3 mL) at room temperature for 3 days

[b]Isolated yield

[c]Anti/syn ratio determined using ^{1}H NMR analysis

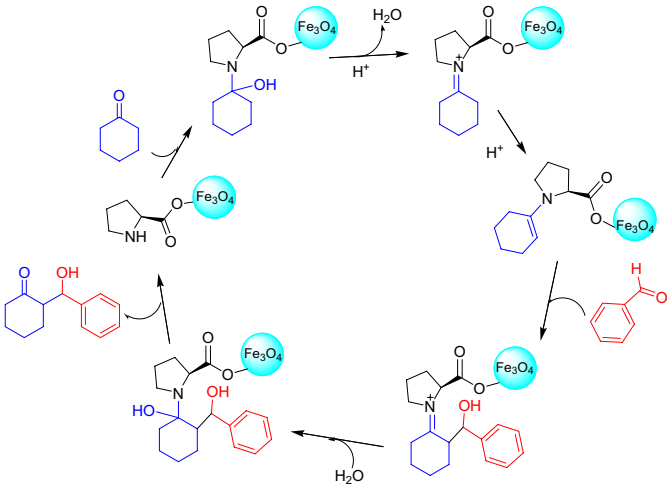


Fig. 9 The proposed mechanism of the aldol reaction catalyzed by **3d**. Note that the different steps are, in principle, reversible, but for clarity, equilibrium arrows are omitted in this figure

acid may proposed to facilitate proton transfers and catalyze the hydrolysis of the iminium intermediate in this reaction mechanism.

Catalyst recovery and reusability

Catalyst recovery and recyclability are of great importance from both practical and environmental perspectives. Therefore, the reusability of the catalyst was investigated using the model reaction between benzaldehyde and cyclohexanone in the presence of 0.03 g of catalyst at room temperature.

The **3c** catalyst could be easily and completely separated from the reaction mixture by applying an external magnetic field. As illustrated in Fig. 10, excellent magnetic separation was achieved upon the application of a simple permanent magnet. After magnetic separation from the reaction mixture, the catalyst was reused in the model reaction for five consecutive cycles. A slight decrease in product yield was observed with each reuse cycle (1st run: 82%; 2nd run: 80%; 3rd run: 79%; 4th run: 78%; 5th run: 76%), indicating good stability and recyclability of the magnetic nanocatalyst.

The recovered catalyst after five cycles was characterized by XRD and FTIR (Fig. S6–S7), showing no significant structural changes compared to the fresh catalyst.

Using the developed methodology, six β-hydroxy ketone derivatives (**4a-4f**) were synthesized via aldol addition reactions between aldehydes (**2a–2c**) and



Fig. 10 Magnetic interaction of the nanocatalyst

ketones **1a** and **1b**. In order to examine electronic effects within the factorial design framework, benzaldehyde derivatives containing electron-donating substituents (Me and OMe) were selected.

Although the electronic variation in this study is limited, the substrate selection was deliberately kept controlled to ensure a balanced and interpretable full factorial design. Incorporating strongly electron-withdrawing or sterically demanding substituents could introduce additional mechanistic complexity, potentially complicating the statistical interpretation of catalyst–substrate interactions.

By focusing on a defined electronic range, the Design of Experiments (DoE) approach allowed clearer evaluation of interaction effects and strengthened the reliability of the statistical analysis. Future studies will expand this methodology to include electronically diverse and sterically hindered substrates to further explore the scope of the catalytic system.

Among the synthesized compounds, three products (**4d, 4e**, and **4f**) are reported here for the first time. All β-hydroxy ketones (**4a-4f**) were obtained in high isolated yields under the selected reaction conditions, demonstrating the effectiveness of the catalytic system within the studied substrate range.

These findings highlight the importance of statistically resolved substrate–catalyst matching in heterogeneous organocatalytic systems and demonstrate the utility of factorial design for mechanistic interpretation of catalytic performance.

Conclusion

In this study, amino acid–functionalized magnetic Fe_3O_4 nanocatalysts were successfully synthesized and applied as efficient and recyclable catalysts for aldol addition reactions. Structural and surface characterization by XRD, FTIR, SEM, EDX, and BET analyses confirmed that the spinel ferrite core structure of Fe_3O_4 was preserved after surface functionalization with L-proline and (2*R*)-2-amino-2-phenylacetic acid.

A systematic full factorial design was employed to evaluate the effects of catalyst type, ketone structure, and aldehyde derivative on reaction yield. Statistical analysis revealed that catalyst identity was the dominant factor governing reaction performance, while strong ketone–catalyst interaction effects highlighted a pronounced substrate–catalyst matching behavior. The developed model exhibited excellent predictive capability ($R^2 = 99.29\%$, $R^2_adj = 97.53\%$, $R^2_pred = 90.84\%$) and was validated through residual diagnostics and experimental verification.

Response optimization identified the combination of cyclohexanone (**1a**), 2-methylbenzaldehyde (**2b**), and Fe_3O_4-L-proline nanocatalyst with benzoic acid addition (**3d**) as the optimal system providing high-performance aldol products under mild conditions. The predicted response was in excellent agreement with experimental results. Moreover, the magnetic nanocatalysts could be readily recovered using an external magnetic field and reused over multiple cycles with only a gradual decrease in catalytic activity.

Using the optimized conditions, a small library of β-hydroxy ketones (**4a-4f**) was synthesized, including three previously unreported compounds, demonstrating the

synthetic applicability of the developed catalytic system. Overall, this work demonstrates that amino acid–functionalized magnetic Fe_3O_4 nanocatalysts, combined with statistical experimental design, provide a practical and reliable platform for the synthesis of aldol-type chemical intermediates.

Supplementary Information The online version contains supplementary material available at https://doi.org/10.1007/s11164-026-05999-w.

Acknowledgements This study has been funded by Istanbul University-Cerrahpaşa, Scientific Research Projects (Project no. FYL-2021-35821).

Author contributions Hasniye Yaşa wrote the main manuscript and Asmar Taghiyeva conducted the experiments. Mustafa Fatih Ergin created the experimental design.

Funding Open access funding provided by the Scientific and Technological Research Council of Türkiye (TÜBİTAK).

Data availability Data is provided within the manuscript or supplementary information files.

Declarations

Conflict of interest The authors declare no competing interests.

Open Access This article is licensed under a Creative Commons Attribution 4.0 International License, which permits use, sharing, adaptation, distribution and reproduction in any medium or format, as long as you give appropriate credit to the original author(s) and the source, provide a link to the Creative Commons licence, and indicate if changes were made. The images or other third party material in this article are included in the article's Creative Commons licence, unless indicated otherwise in a credit line to the material. If material is not included in the article's Creative Commons licence and your intended use is not permitted by statutory regulation or exceeds the permitted use, you will need to obtain permission directly from the copyright holder. To view a copy of this licence, visit http://creativecommons.org/licenses/by/4.0/.

References

1. M. Kooti, F. Kooshki, E. Nasiri, Preparation and characterization of magnetic graphene nanocomposite containing Cu(proline)$_2$ as catalyst for asymmetric aldol reactions. Res. Chem. Intermed. **45**, 2641–2656 (2019)
2. A.M. Abu-Dief, S.M. Abdel-Fatah, Development and functionalization of magnetic nanoparticles as powerful and green catalysts for organic synthesis. Beni-Suef Univ. J. Basic Appl. Sci. **7**, 55–67 (2018)
3. G.G. Hawley, R.J. Lewis, *Hawley's condensed chemical dictionary*, 14th edn. (Wiley, NY, 2001), p.1630
4. T. Yıldız, H. Can, A.S. Yusufoğlu, An effective and environmentally friendly synthesis of 1,3-keto-alcohols. Org. Prep. Proced. Int. **52**, 9–21 (2020)
5. J.P. Guthrie, Rate-equilibrium correlations for the aldol condensation: an analysis in terms of Marcus theory. J. Am. Chem. Soc. **113**, 7249–7255 (1991)
6. T. Yıldız, H. Yaşa, B. Hasdemir, A.S. Yusufoğlu, Different bio/Lewis acid-catalyzed stereoselective aldol reactions in various mediums. Monatsh. Chem. **148**, 1445–1452 (2017)
7. T. Yıldız, B. Hasdemir, H. Yaşa, H. Başpınar Küçük, New strategy for the synthesis of some valuable chiral 1,3-diols with high enantiomeric purity: new organocatalyst, asymmetric aldol reaction, and reduction. ACS Omega **9**, 12657–12664 (2024)

8. T. Yıldız, An enzymatic and environmentally friendly route for the synthesis of chiral β-hydroxy ketones. ChemistrySelect **4**, 7927–7931 (2019).
9. P.T. Anastas, J.C. Warner, *Green Chemistry: Theory and Practice*, revised ed. (Oxford University Press, 2000), p.152
10. N. Winterton, News and views. Green Chem. **3**, G73–G81 (2001)
11. A.D. Curzons, D.N. Mortimer, D.J.C. Constable, V.L. Cunningham, So you think your process is green, how do you know? — using principles of sustainability to determine what is green – a corporate perspective. Green Chem. **3**, 1–6 (2001)
12. M. Eissen, J.O. Metzger, E. Schmidt, U. Schneidewind, 10 years after Rio-concepts on the contribution of chemistry to a sustainable development. Angew. Chem. Int. Ed. **41**, 414–436 (2002)
13. M. Eissen, J.O. Metzger, Environmental performance metrics for daily use in synthetic chemistry. Chem. Eur. J. **8**, 3580–3585 (2002)
14. M. Eissen, R. Mazur, H. Quebbemann, K. Pennemann, Atom economy and yield of synthesis sequences. Helv. Chim. Acta **87**, 524–535 (2004)
15. M. Lancaster, Green chemistry: An Introductory Text. Book and Media Reviews, ed. by J. Kovac (Royal Society of Chemistry, Cambridge, 2002)
16. M. Lancaster, Principles of sustainable and green chemistry, in *Handbook of Green Chemistry and Technology*. ed. by J.H. Clark, D. Macquarrie (Wiley, 2002), p.25
17. V. Polshettiwar, R. Luque, A. Fihri, H. Zhu, M. Bouhrara, J.M. Basset, Magnetically recoverable nanocatalysts. Chem. Rev. **111**, 3036–3075 (2011)
18. S. Shylesh, V. Schünemann, W.R. Thiel, Magnetically separable nanocatalysts: bridges between homogeneous and heterogeneous catalysis. Angew. Chem. Int. Ed. **49**, 3428–3459 (2010)
19. Y. Chi, Q. Yuan, Y. Li, J. Tu, l Zhao, N. Li, X. Li, Synthesis of Fe_3O_4@SiO_2–Ag magnetic nanocomposite based on small-sized and highly dispersed silver nanoparticles for catalytic reduction of 4-nitrophenol. J. Colloid Interface Sci. **383**, 96–102 (2012)
20. Y. Deng, Y. Cai, Z. Sun, D. Zhao, Magnetically responsive ordered mesoporous materials: a burgeoning family of functional composite nanomaterials. Chem. Phys. Lett. **510**, 1–13 (2011)
21. A.M. Balu, B. Baruwati, E. Serrano, J. Cot, J. Garcia-Martinez, R.S. Varma, R. Lugue, Magnetically separable nanocomposites with photocatalytic activity under visible light for the selective transformation of biomass-derived platform molecules. Green Chem. **13**, 2750–2758 (2011)
22. S. Angela, M. Ludmila, I. Cornelia-Ioana, F. Denisa, C. Cristina, P. Natalia, G. Sabina, M. Mateusz, K. Joanna, S. Adrian-Vasile, T.D. Roxana, O.O. Cristian, F. Anton, Aminoacid functionalised magnetite nanoparticles Fe_3O_4@AA (AA = Ser, Cys, Pro, Trp) as biocompatible magnetite nanoparticles with potential therapeutic applications. Sci. Rep. **14**, 26228 (2024)
23. J. Safaei-Ghomi, S. Zahedi, L -Proline-functionalized Fe_3O_4 nanoparticles as a novel magnetic chiral catalyst for the direct asymmetric Mannich reaction. Appl. Organomet. Chem. **29**, 566–571 (2015)
24. A.A. Dar, P. Yadav, A. N, T.W. A, Optimizing processes and products: the role of DOE. Insight – Statistics **7**(1), 644 (2024)
25. M. Motaln, T. Lerher, Innovative approaches to wear reduction in horizontal powder screw conveyors: a design of experiments-guided numerical study. Appl. Sci. (Basel) **14**, 3064 (2024)
26. H. Yaşa, M.F. Ergin, A. Ergin, G. Alkan, Importance of inert gases for chemical transportation. Proc. Book **10**, 825 (2016)
27. D. C. Montgomery, Design and Analysis of Experiments, 9th edn. (Wiley, 2017)
28. H. Çelik Onar, M.F. Ergin, H. Yaşa, Investigating the role of citric acid as a natural acid on the crystallization of amoxicillin trihydrate. ACS Omega **8**, 36344–36354 (2023)
29. H. Yaşa, M.F. Ergin, H. Çelik Onar, Guiding role and optimization of malic acid in the crystallization of amoxicillin trihydrate. Can. J. Chem. Eng. **103**, 6151–6165 (2025)
30. H.B. Kucuk, G. Kanturk, S. Yerlikaya, T. Yildiz, A.M. Senturk, M. Guzel, Novel β-hydroxy ketones: synthesis, spectroscopic characterization, molecular docking, and anticancer activity studies. J. Mol. Struct. **1250**, 131772 (2022)
31. Y.S. Marya, L. Ushakumari, B. Harikumar, H.T. Varghese, C.Y. Panicker, FT-IR, FT-raman and SERS spectra of L-proline. JICS **6**, 138–144 (2009)
32. I. Ahmad, A. Abbasi, Z.M. El Bahy, S. Ikram, Synergistic effect of silver NPs immobilized on Fe3O4@L-proline magnetic nanocomposite toward the photocatalytic degradation of Victoria blue and reduction of organic pollutants. Environ. Sci. Pollut. Res. Int. **30**, 78891–78912 (2023)
33. J.M. Lehn, *Supramolecular Chemistry: Concepts and Perspectives, Supramolecular Chemistry: Concepts and Perspectives*, First edn. (Wiley, 1995), pp.1–271

34. R. Leardi, Experimental design in chemistry: a tutorial. Anal. Chim. Acta **652**, 161–172 (2009)
35. P.H.Y. Cheong, C.Y. Legault, J.M. Um, N. Çelebi-Ölçüm, K.N. Houk, Quantum mechanical investigations of organocatalysis: mechanisms, reactivities, and selectivities. Chem. Rev. **111**, 5042–5137 (2011)
36. A.G. Doyle, E.N. Jacobsen, Small-molecule H-bond donors in asymmetric catalysis. Chem. Rev. **107**, 5713–5743 (2007)
37. M.S. Taylor, E.N. Jacobsen, Asymmetric catalysis by chiral hydrogen-bond donors. Angew. Chem. Int. Ed. **45**, 1520–1543 (2006)
38. A.S. Mahadevi, G.N. Sastry, Cooperativity in noncovalent interactions. Chem. Rev. **116**, 2775–2825 (2016)
39. M. Edin, J.E. Bäckvall, A. Córdova, Tandem enantioselective organo- and biocatalysis: a direct entry for the synthesis of enantiomerically pure aldols. Tetrahedron Lett. **45**, 7697–7701 (2004).
40. A. Córdova, W. Zou, P. Dziedzic, I. Ibrahem, E. Reyes, Y. Xu, Direct asymmetric intermolecular aldol reactions catalyzed by amino acids and small peptides. Chem. Eur. J. **12**, 5383–5397 (2006)
41. Y. Hayashi, T. Itoh, N. Nagae, M. Ohkubo, H. Ishikawa, The effectiveness of proteinogenic amino acids in the asymmetric aldol reaction in DMSO and aqueous DMSO. Synlett **10**, 1565–1570 (2008)
42. G. E. P. Box, J. S. Hunter, W. G. Hunter, Statistics for experimenters: design, innovation, and discovery. 2nd edn. (Wiley-Interscience, 2005)

Publisher's Note Springer Nature remains neutral with regard to jurisdictional claims in published maps and institutional affiliations.

Authors and Affiliations

Asmar Taghiyeva[1] · Hasniye Yaşa[2] · Mustafa Fatih Ergin[3]

✉ Hasniye Yaşa
hasniye@iuc.edu.tr

[1] Institute of Graduate Studies, Istanbul University-Cerrahpaşa, 34320 Istanbul, Turkey

[2] Department of Chemistry, Faculty of Engineering, Istanbul University-Cerrahpaşa, 34320 Istanbul, Turkey

[3] Faculty of Engineering, Chemical Engineering, Istanbul University-Cerrahpaşa, 34320 Istanbul, Turkey